iScience

CellPress

Article

Identifying Mn^{VII}-oxo Species during Electrochemical Water Oxidation by Manganese Oxide

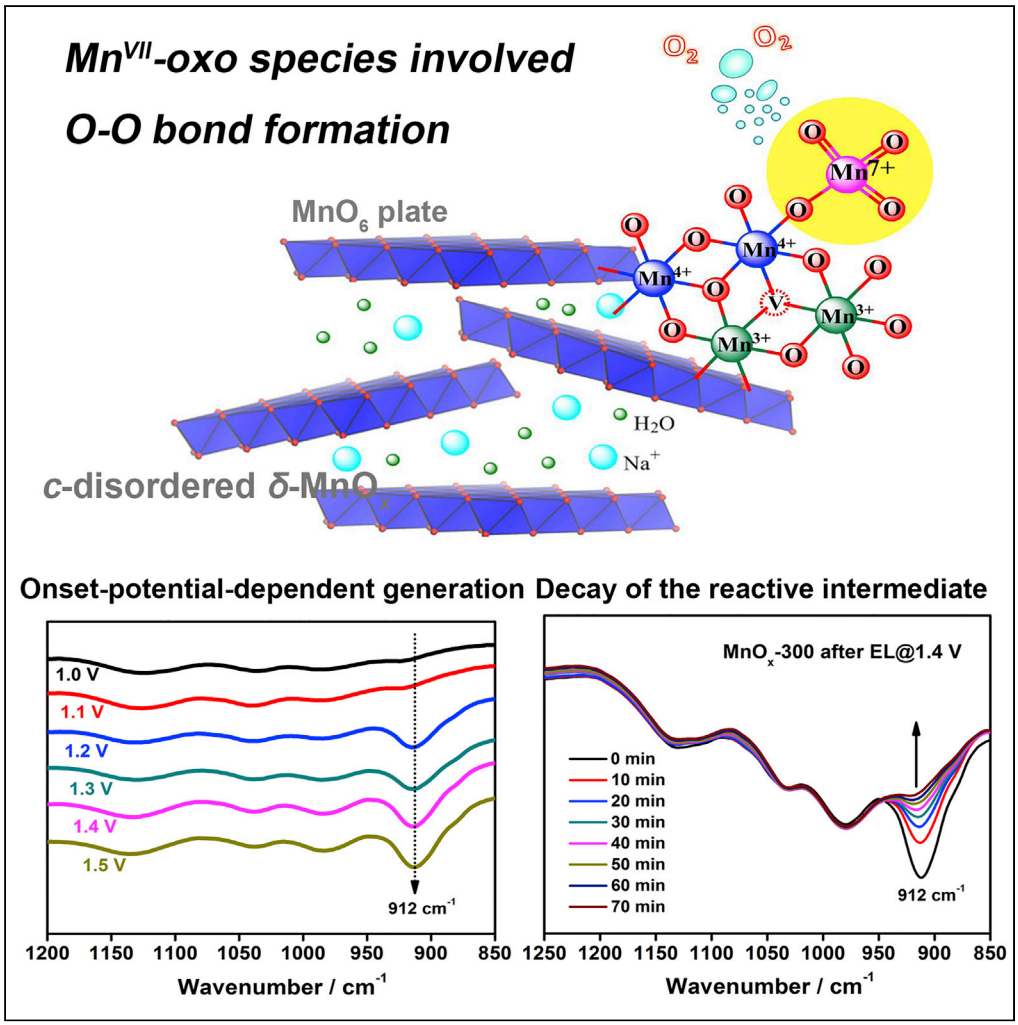

Biaobiao Zhang, Quentin Daniel, Lizhou Fan, Tianqi Liu, Qijun Meng, Licheng Sun

lichengs@kth.se

HIGHLIGHTS

A reactive Mn^{VII}-oxo intermediate was identified during water oxidation by a MnO_x

The Mn^{VII}-oxo species was proved to be much more oxidative than permanganate ion

The Mn^{IV}–O–Mn^{VII} = O moiety is a real highly active state for O–O bond formation

A new mechanism for Mn oxide-catalyzed electrocatalytic water oxidation is proposed

Zhang et al., iScience 4, 144–152
June 29, 2018
https://doi.org/10.1016/j.isci.2018.05.018

iScience

CellPress

Article

Identifying Mn^{VII}-oxo Species during Electrochemical Water Oxidation by Manganese Oxide

Biaobiao Zhang,[1] Quentin Daniel,[1] Lizhou Fan,[1] Tianqi Liu,[1] Qijun Meng,[1] and Licheng Sun[1,2,3,*]

SUMMARY

Identifying surface active intermediate species is essential to reveal the catalytic mechanism of water oxidation by metal-oxides-based catalysts and to develop more efficient catalysts for oxygen-oxygen bond formation. Here we report, through electrochemical methods and *ex situ* infrared spectroscopy, the identification of a Mn^{VII} = O intermediate during catalytic water oxidation by a *c*-disordered δ-MnO_x with an onset-potential-dependent reduction peak at 0.93 V and an infrared peak at 912 cm^{-1}. This intermediate is proved to be highly reactive and much more oxidative than permanganate ion. Therefore, we propose a new catalytic mechanism for water oxidation catalyzed by Mn oxides, with involvement of the Mn^{VII} = O intermediate in a resting state and the Mn^{IV}–O–Mn^{VII} = O as a real active species for oxygen-oxygen bond formation.

INTRODUCTION

The continuous extraction of electrons and protons from water is a key step in sustaining life on Earth, and research on such processes is crucial for developing renewable energy systems via artificial photosynthesis (Walter et al., 2010). In nature, water oxidation occurs at the Mn_4CaO_5 cluster in photosystem II (PSII), with a low overpotential of around 160 mV and high rate of 100–400 s^{-1}(Cox et al., 2013; Najafpour et al., 2016; Umena et al., 2011; Limburg et al., 1999). Although Mn complexes and oxides have been developed as promising water-oxidation catalysts (WOCs) (Najafpour et al., 2016; Limburg et al., 1999), the activity gaps between artificial catalysts and the Mn_4CaO_5 cluster are large (Najafpour et al., 2016). One primary reason for the ineffectual development of Mn-based WOCs is our limited understanding of the water-oxidation mechanism in PSII. In conventional mechanistic models, Mn^{IV} = $O^{\bullet}$ and Mn^{V} = O species are widely accepted as key intermediates for both Mn_4CaO_5 clusters and synthetic catalysts (Cox et al., 2013; Zahran et al., 2016; Najafpour et al., 2016; Jin et al., 2017). However, these mechanisms do not reflect the unique redox chemistry of Mn (five valences, varying from Mn^{II} to Mn^{VII}, incorporation of many disproportionation and comproportionation reactions, moderate oxidation potentials from Mn^{II} to Mn^{VII}) and the fact that low-valent Mn^{III} species and high-valent MnO_4^- species are usually observed during water-oxidation catalysis (Takashima et al., 2012; Yagi and Narita, 2004; Limburg et al., 1997, 1999). Significant improvements in the catalytic performance of Mn-based WOCs could be aided by the exploration of more appropriate catalytic mechanisms for Mn-based catalysts. Here, we report the first direct experimental evidence for the formation of a Mn^{VII} = O intermediate during catalytic water oxidation on a *c*-disordered δ-MnO_x, MnO_x-300, which was previously developed by our group (Zhang et al., 2017). On the basis of this discovery, an innovative water-oxidation mechanism that involves Mn^{VII} = O is proposed. This new information on water oxidation with a Mn-based catalyst might help designing more efficient Mn-based WOCs for artificial photosynthesis.

RESULTS

Observation of an Intermediate State at 0.93 V by Electrochemical Study

The cyclic voltammetry (CV) curve of MnO_x-300 (Figure 1A) shows that as the potential increases, the MnO_x-300 film is gradually oxidized. When the potential approaches the water-oxidation onset potential, at around 1.1 V (Zhang et al., 2017), the active Mn sites are oxidized to a high oxidation state, followed by the evolution of oxygen. There are no distinct oxidation peaks, and only one broad wave is observed before the initiation of water oxidation at around 1.1 V versus the normal hydrogen electrode (NHE), indicating the presence of strong electronic interactions between Mn sites in MnO_x-300 (Zaharieva et al., 2012). This high oxidation state of MnO_x-300, which does not give distinct oxidation peaks, is completely unexpected. High

[1]Department of Chemistry, KTH Royal Institute of Technology, Stockholm 10044, Sweden

[2]State Key Laboratory of Fine Chemicals, Institute of Artificial Photosynthesis, DUT-KTH Joint Education and Research Center on Molecular Devices, Dalian University of Technology (DUT), Dalian 116024, P. R. China

[3]Lead Contact

*Correspondence: lichengs@kth.se

https://doi.org/10.1016/j.isci.2018.05.018

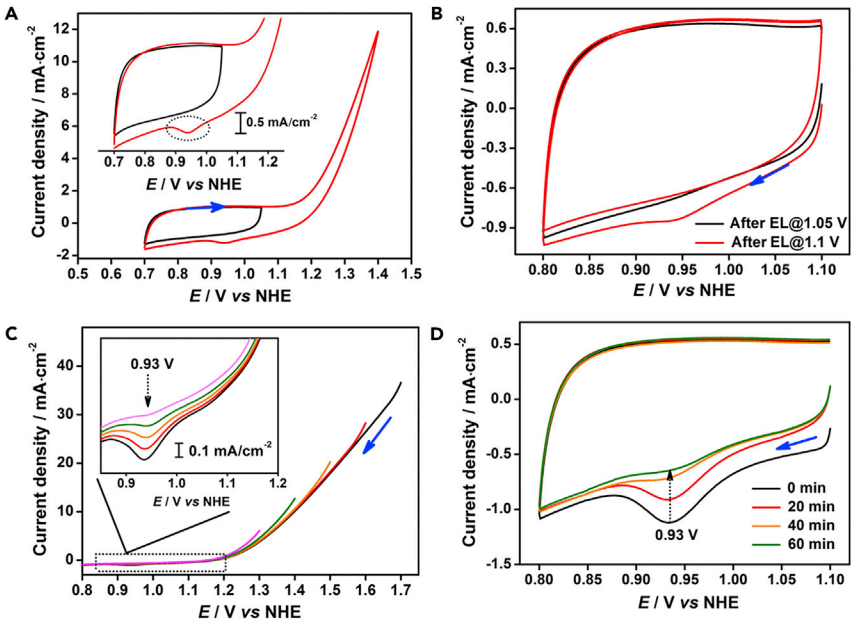

Figure 1. Observation of Intermediate State at 0.93 V vs Normal Hydrogen Electrode (NHE) by Cyclic Voltammetry (CV)

(A) CV curves of MnO_x-300 in two different potential regions. The inset shows enlarged CV curves.

(B) Negative-scan CV curves of MnO_x-300 after electrolysis at 1.05 V and 1.1 V for 10 min

(C) Negative-scan linear sweep voltammetry (LSV) curves swept from 1.7 V (black curve), 1.6 V (red curve), 1.5 V (orange curve), 1.4 V (green curve), and 1.3 V (magenta curve). The inset shows enlarged parts of the LSV curves.

(D) Negative-scan CV curves of MnO_x-300 after electrolysis at 1.4 V for 2 min with different delay times. The MnO_x-300 electrode was removed after electrolysis, quickly rinsed with water, and dried in a N_2 flow. It was then kept under air for 20, 40, and 60 min, respectively, before the CV was recorded. Electrolyte was 1.0 M KPi (pH 7). Scan rate was 10 mV/s. Blue arrows show scan direction.

See also Figures S1–S4.

oxidation states, such as Mn^{IV}, Mn^{V}, Mn^{VI}, and Mn^{VII} species, may be possible intermediates involved in this state.

However, we observed a distinct reduction peak at 0.93 V during a negative scan; this peak does not appear when the potential is swept in the range 0.7–1.05 V, in which water oxidation does not occur (Figure 1A). In addition, there is no evident reduction peak in the potential region 0.7–1.5 V in the CV curve of MnO_x-300 in a CH_2Cl_2 electrolyte, in which no water is present (Figure S1). Figure 1B shows that the peak at 0.93 V appears in the first cycle in the CV curve of MnO_x-300 after electrolysis (EL) at 1.1 V, at which water oxidation is initiated (Zhang et al., 2017). The reduction peak vanishes in the second cycle because the relevant species were reduced during the first scan. In contrast, no reduction peak is observed for MnO_x-300 after electrolysis at 1.05 V. The negative-scan linear sweep voltammetry (LSV) curves in Figure 1C show that the increment in the current intensity of the peak at 0.93 V is consistent with the increase in the catalytic current density with increasing LSV initial potential.

These results clearly show that the reduction peak at 0.93 V is attributable to the reduction of an active intermediate state, and its generation strictly corresponds to initiation of the water-oxidation reaction. We further found that the intermediate state rapidly and repeatedly accumulates in MnO_x-300 after electrolysis at 1.4 V, at which voltage catalytic water oxidation is fast (Figures S2–S4). Figure 1D shows that complete degradation of the generated active intermediate state occurred in a period of 60 min; this can be considered as its lifetime under the experimental conditions.

Observation of the Intermediate State at 912 cm^{-1} by Infrared Spectroscopy

The lifetime of the observed intermediate state is on a 1 hr timescale; therefore it is possible to identify the structure of the intermediate by *ex situ* attenuated total reflection Fourier transform infrared (ATR-FTIR)

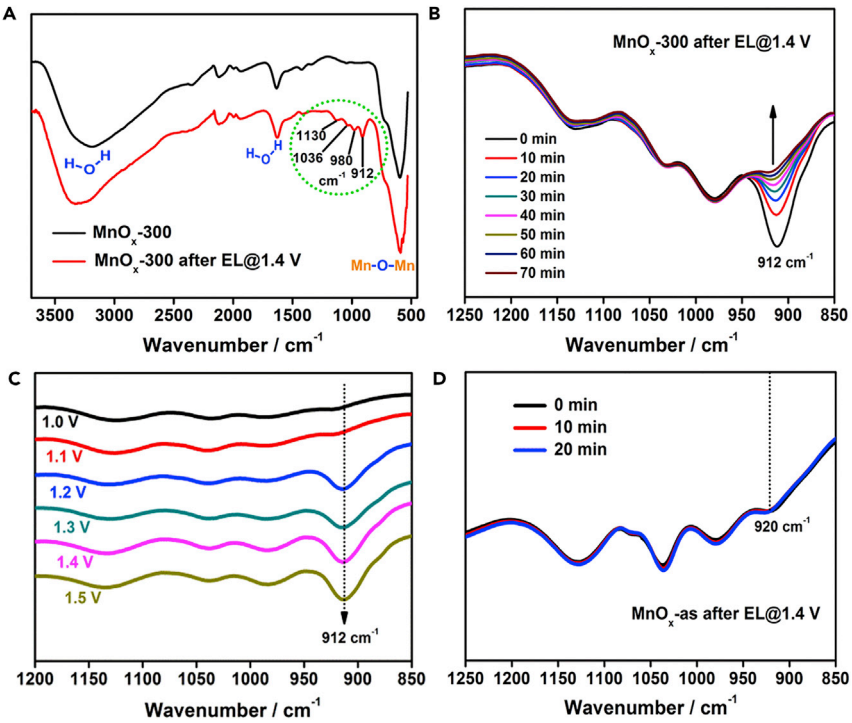

Figure 2. Observation of Intermediate State at 912 cm^{-1} by IR Spectroscopy

(A) IR spectra of pristine MnO_x-300 and MnO_x-300 after electrolysis at 1.4 V.

(B) Time-resolved IR spectra of MnO_x-300 after electrolysis at 1.4 V. During the aging period, the sample was just kept on the sample holder without any other operation.

(C) IR spectra of MnO_x-300 after electrolysis at different potentials.

(D) Time-resolved IR spectra of MnO_x-as after electrolysis at 1.4 V.

See also Figures S5–S7.

spectroscopy, which has been successfully employed to identify surface active species on metal oxides, such as Co_3O_4 and Fe_2O_3 (Zandi and Hamann, 2016; Zhang et al., 2014). Compared with the infrared (IR) spectrum of pristine MnO_x-300, four new IR peaks, at 1130, 1036, 980, and 912 cm^{-1}, were observed in the spectrum of MnO_x-300 after electrocatalysis at 1.4 V (Figure 2A). The first three peaks are assigned to either or both physisorbed and coordinated phosphate groups, because these peaks are invariable (Figure 2B), potential independent (Figures 2C and S5), and consistent with the IR absorption peaks of potassium phosphates (Figure S6). The absorption peak at 912 cm^{-1} gradually vanishes within 60 min (Figure 2B) and appears only when the applied potential is higher than the water-oxidation onset potential (Figure 2C). We already found that the reduction peak at 0.93 V completely vanished after the first cycle of the negative CV scan (Figures 1B and S2). Consistent with this, no 912 cm^{-1} peak was observed in the IR spectrum of MnO_x-300 after electrocatalysis followed by a negative CV scan (Figure S7). In addition, given the consistency in the degradation rate and the potential-dependent generation between the 912 cm^{-1} peak and the reduction peak at 0.93 V, it is reasonable to attribute the 912 cm^{-1} peak to the same active intermediate state as that observed in the above-mentioned electrochemical study.

To confirm that the observed intermediate state is essentially involved in water oxidation catalyzed by MnO_x-300, we investigated the precursor of MnO_x-300, denoted by MnO_x-as, which has no catalytic activity in water oxidation (Zhang et al., 2017). The IR peak at 912 cm^{-1} was absent from the IR spectrum of MnO_x-as after electrolysis at 1.4 V (Figure 2D). The spectrum showed only one small and invariable peak, at 920 cm^{-1}, which can be attributed to phosphate groups, implying that the active intermediate state is not generated on the inactive MnO_x-as. These results confirm the discovery of an active intermediate state with a reduction peak at 0.93 V and IR peak at 912 cm^{-1} for the MnO_x-300-based WOC. The intermediate state is reactive, and its generation strictly corresponds to water-oxidation catalysis, i.e., it is involved in the catalytic cycle.

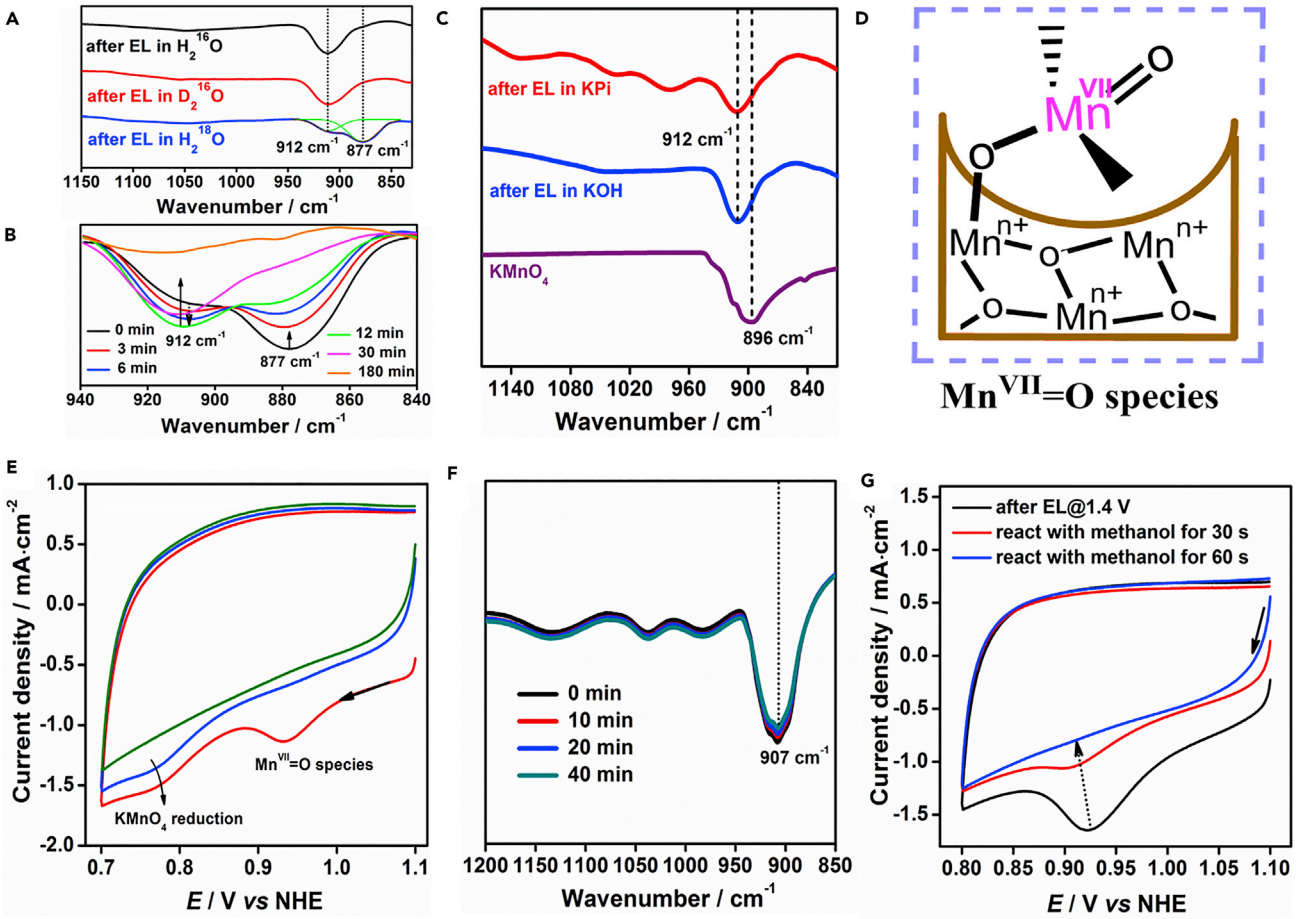

Figure 3. Investigation of the Nature of the Observed Intermediate State and Distinctions between its Reactivity and that of $KMnO_4$

(A) IR spectra of MnO_x-300 after electrolysis at 0.85 V in $H_2{}^{16}O$, $D_2{}^{16}O$, and $H_2{}^{18}O$ KOH electrolyte.

(B) Time-resolved IR spectra of MnO_x-300 after electrolysis at 1.4 V in $H_2{}^{18}O$ KOH electrolyte.

(C) Comparison of IR spectra of $KMnO_4$ and MnO_x-300 after electrolysis at 1.4 V in 1.0 M KPi solution and at 0.85 V in 1.0 M KOH electrolyte.

(D) Schematic diagram of suggested structure of observed intermediate species.

(E) Negative-scan CV curves of MnO_x-300 after electrolysis at 1.4 V in 1.0 M KPi electrolyte with 1 mM $KMnO_4$ (the red curve is the first cycle, and the blue curve is the second cycle). The green curve is the second cycle of the CV curve of MnO_x-300 after electrolysis at 1.4 V in 1.0 M KPi electrolyte without $KMnO_4$.

(F) Time-resolved IR spectra of $KMnO_4$ associated with MnO_x-300.

(G) Negative-scan CV curves of MnO_x-300 after electrolysis at 1.4 V, followed by reaction with CH_3OH for different reaction times.

See also Figures S8–S15.

The Nature of the Observed Intermediate State

Isotopic IR spectroscopic analysis was performed to facilitate assignment of the IR absorption bands of the observed intermediate state. To eliminate overlapping of the IR absorptions of phosphate groups, the catalytic reaction with MnO_x-300 was performed in a KOH solution (see Transparent Methods and Figures S8–S11). The 912 cm^{-1} peak did not shift on substitution of H_2O with D_2O in the electrolyte solution, which shows that −OH is not involved in the structure of this intermediate state (Figure 3A). For MnO_x-300 after electrolysis in $H_2{}^{18}O$ electrolyte, a strong isotopic counterpart at 877 cm^{-1} of the 912 cm^{-1} peak appeared, i.e., an isotopic shift of 35 cm^{-1}, suggesting that the surface intermediate species has O in its structure. The time-resolved changes in the multiple isotopic peaks are shown in Figure 3B. In the first 12 min, the intensity of the 877 cm^{-1} peak decreased rapidly and that of the 912 cm^{-1} peak grew significantly. After 30 min, the 877 cm^{-1} peak became indistinct and the 912 cm^{-1} peak intensity decreased compared with that of the peak at 12 min. Both peaks vanished after 180 min. This demonstrates that the O atoms in the intermediates exchange rapidly with either or both atmospheric water and oxygen. This further proves that the intermediate is in a very reactive state.

In previous studies, several species, including Mn^{IV} = O, Mn^{V} = O, Mn–O–O, and Mn–O–OH, have been identified in the intermediate states of manganese oxide-based WOCs (Zahran et al., 2016; Najafpour et al., 2016; Jin et al., 2017). However, the vibration frequency of the MnO_x-300 intermediate cannot be attributed to any of these species, because the vibration frequencies of Mn^{IV} = O (Chu et al., 2001; Czernuszewicz et al., 1988), Mn^{V} = O (Chu et al., 2001; Workman et al., 1992), and superoxide-like Mn species (Che and Tench, 1983; Baltanas et al., 1984) generally fall in the region 712–755 cm^{-1}, 970–981 cm^{-1}, and 1075–1195 cm^{-1}, respectively, which are far from the observed vibration frequency, i.e., 912 cm^{-1}. Unexpectedly, the 912 cm^{-1} peak closely matches the IR absorption of $KMnO_4$, which is at 896 cm^{-1} (Figure 3C). Moreover, an ^{18}O isotopic shift of 34 cm^{-1} for $KMnO_4$ has been reported (Dong et al., 2002), which is in good agreement with the detected 35 cm^{-1} shift for the intermediates. We observed MnO_4^- release from the surface of the MnO_x electrode during the first tens of seconds of electrolysis at 1.4 V, but it vanished within a minute (Video S1 and Figure S12). We therefore propose that the active intermediate state consists of a Mn^{VII} = O species bonded to the positively charged surface of MnO_x-300 (Figure 3D).

To clarify the nature of the identified intermediate, we investigated five lines of experimental evidence to distinguish it from free MnO_4^-, which is usually a corrosive by-product during water oxidation with Mn catalysts (Limburg et al., 1997, 1999; Yagi and Narita, 2004). The first two direct differences between the Mn^{VII} = O species and MnO_4^- are the shifts of the CV reduction peak and the IR absorption peak. In addition to the expected reduction of the Mn^{VII} = O species at 0.93 V, another peak, at 0.77 V, which still remained in the second cycle of the negative CV scan, was observed, as shown in Figure 3E. The latter peak clearly corresponds to the reduction of $KMnO_4$ in the electrolyte. The higher reduction potential of the Mn^{VII} = O species than that of MnO_4^- shows that the oxidative reactivity of the Mn^{VII} = O species is much higher than that of MnO_4^-. The IR peak of the Mn^{VII} = O species is red shifted by 16 nm compared with that of $KMnO_4$ (Figure 3C). A similar red shift of the IR peak has been reported for $KMnO_4$ adsorbed on β-MnO_2 (Abbas and Nasser, 2000). This supports the hypothesis that the intermediate species is a Mn^{VII} = O species bound on a MnO_x nanostructure.

The third argument is the specific degradation of the Mn^{VII} = O species, shown in Figure 2B. To achieve a better comparison with the generated Mn^{VII} = O species, $KMnO_4$ was drop-cast on a MnO_x-300 sample after electrolysis at 1.4 V for 20 min and a negative-scan CV was then performed to remove the generated Mn^{VII} = O species. After drying, the mixture was collected for IR spectroscopy. No significant degradation was observed in a mixture of $KMnO_4$ and the processed MnO_x-300 (Figure 3F). The observed fast ^{18}O exchange of the intermediate in Figure 3B is the fourth solid piece of evidence, because $KMnO_4$ does not exchange with ambient oxygen at room temperature (Yiu et al., 2011; Shafirovich et al., 1981). Rapid O exchange with ambient oxygen occurs only for some activated MnO_4^- species, such as $[2BF_3 \cdot MnO_4]^-$ species (Yiu et al., 2011), and a Mn^{IV}–Mn^{VII} surface complex (Shafirovich et al., 1981). Direct investigation of the oxidative reactivity of our Mn^{VII} = O intermediate species is the fifth probe (see Transparent Methods and Figures S13–S15). It has been reported that $KMnO_4$ can oxidize CH_3OH at room temperature but the reaction rate is extremely slow, unless the $KMnO_4$ is activated by a strong Lewis acid (Du et al., 2011). Here, we found that the degradation of our Mn^{VII} = O species in CH_3CN with 0.1 M CH_3OH was complete within 1 min (Figure 3G). In contrast, the degradation of $KMnO_4$ under the same conditions was negligible even after 6 hr (Figure S15).

These results fully demonstrate that the identified Mn^{VII} = O species is a disparate species with a reactivity much higher than that of free MnO_4^-. The higher reactivity of the Mn^{VII} = O species can be attributed to its bonding to the charged bulk surface, which acts similarly to a Lewis acid, which has been proved to significantly enhance the oxidative reactivity of MnO_4^- (Du et al., 2011; Yiu et al., 2011).

DISCUSSION

On the basis of these results, we could propose a catalytic water-oxidation mechanism that involves Mn^{VII} = O. However, we first have to address two essential questions.

The first question is what are the rationale and pathway for the formation of Mn^{VII} = O species on δ-MnO_x under such a low potential? In Pourbaix diagrams for Mn, δ-MnO_x borders the MnO_4^- zone (Izgorodin et al., 2012; Najafpour et al., 2016). At pH 7, the theoretical potential for the formation of

MnO_4^- is 1.05 V. With an overpotential of 50 mV, it is thermodynamically possible to generate Mn^{VII} species in MnO_x-300 at 1.1 V. Regarding the formation pathway, it has been found that four Mn^{IV} ions can disproportionate into one Mn^{VII} ion and three Mn^{III} ions via a tetranuclear Mn^{IV} intermediate species (Shafirovich et al., 1981; Dzhabiev, 1989). Furthermore, kinetic analysis has shown that two molecules of $[(H_2O)(tpy)Mn(\mu\text{-}O)_2Mn(tpy)(H_2O)]$ (tpy = 2,2′:6′,2″-terpyridine), i.e., four Mn cores, are involved in the rate-determining step of the formation of MnO_4^- (Yagi and Narita, 2004; Limburg et al., 1999). Strong electronic interactions between Mn sites in MnO_x-300 before the generation of the Mn^{VII} = O sites were also observed in positive scans of MnO_x-300 (see Figure 1A) (Zaharieva et al., 2012). On the basis of these information and our observations, we propose that, in the formation of the Mn^{VII} = O species, multiple Mn sites (both the active Mn site and its surrounding Mn) participate in the process and a complicated disproportionation reaction such as $Mn^{IV}Mn^{IV}Mn^{IV}Mn^{IV}$ to $Mn^{VII}Mn^{III}Mn^{III}Mn^{III}$ may be involved.

The second question is what is the thermodynamic and kinetic feasibility of oxygen evolution from Mn^{VII} = O species? Looking again at the Pourbaix diagrams, $E(MnO_4^-/\delta\text{-}MnO_x) \approx 1.05$ V at pH 7; this is 230 mV higher than the thermodynamic potential for water oxidation. MnO_4^- can therefore spontaneously oxidize H_2O to O_2 under neutral conditions via Equation 1 (Skrabal, 1910).

$$4MnO_4^- + 2H_2O \rightarrow 4MnO_2 + 3O_2 + 4OH^- \qquad \text{(Equation 1)}$$

Although the rate of oxygen evolution from free MnO_4^- is very slow, it has been reported that the rate increases significantly if MnO_4^- is bonded with MnO_2, a Mn^{4+} ion, or a Lewis acid (Skrabal, 1910; Yiu et al., 2011; Shafirovich et al., 1981). It has been known since 1910 that MnO_2 catalyzes the reaction of MnO_4^- with H_2O (Skrabal, 1910). Shafirovich et al. studied the kinetics of the reaction of MnO_4^- with H_2O, with Mn^{4+} as a catalyst. They suggested that a Mn^{IV}–Mn^{VII} surface complex is the key intermediate for O–O formation in the catalytic mechanism (Figure 4A) (Shafirovich et al., 1981; Shafirovich, 1978). The crystal structure of a $(H_3O)_2$–$[Mn^{IV}(Mn^{VII}O_4)_6]\cdot 11H_2O$ intermediate complex, which rapidly evolves oxygen at $T \geq -4°C$, has been identified by Krebs and Hasse (Figure 4B) (Krebs and Hasse, 1974). Recently, a highly active pendant Mn^{VII} = O moiety on a cubic Mn–nitride complex was suggested as a synthetic structural model of the proposed S4 state in PSII (Figure 4C) (Vaddypally et al., 2017). The work by Lau's group shows that MnO_4^- activated by a strong Lewis acid, namely, BF_3, rapidly evolves O_2 via intramolecular coupling of two Mn–oxo species (Figure 4D) (Yiu et al., 2011). A Mn^{VII}–nitrido complex was also reported by the same group as an essential intermediate in Ce^{IV}-driven water oxidation (Ma et al., 2015). All these previous reports suggest that oxygen evolution at a Mn^{VII} = O site bonded to an oxidized cluster is not only thermodynamically possible but also has rapid kinetics.

Finally, we propose a catalytic cycle that involves Mn^{VII} = O for water-oxidation catalysis by MnO_x-300 (Figure 4E). One active Mn site and three related Mn atoms are assumed to participate actively in the catalysis. After multiple charge accumulation accompanied by transfer of three electrons and two protons, the initial state, i.e., $[Mn^{III}Mn^{III}Mn^{IV}(HO{-}Mn^{III}{-}OH_2)]$ (S_0), is oxidized to $[Mn^{IV}Mn^{IV}Mn^{IV}(HO{-}Mn^{IV}=O)]$ (S_3) via states S_1 and S_2. State S_3 is assumed to be a transition state, which will undergo charge rearrangement with the release of one proton, resulting in a resting state, $[Mn^{III}Mn^{III}Mn^{III}Mn^{VII}(=O)_2]$ (S_4), which probably contains a dangling Mn^{VII} = O site. The observed CV reduction peak at 0.93 V and the IR absorption frequency of 912 cm^{-1} can be related to this Mn^{VII} = O site in S_4. Before O–O bond formation, the Mn atom directly bonded to the dangling Mn^{VII} = O site is thought to be further oxidized to Mn^{IV}, which acts as a strong Lewis acid and promotes the reactivity of the Mn^{VII} = O site, forming the active state $[Mn^{III}Mn^{III}Mn^{IV}Mn^{VII}(=O)_2]$ (S_4'). Along with oxygen evolution from S_4', the involved Mn cluster returns to its starting state S_0 by binding two H_2O molecules to the empty sites and losing one proton, completing one catalytic cycle. Finally, we would like to point out that the commonly observed essential Mn^{III} species is probably formed in the charge rearrangement step and the corrosive product MnO_4^- is probably formed by the detachment of the Mn^{VII} = O site from either or both S_4 and S_4', because the $Mn^{IV}{-}O$ bond in the $Mn^{IV}{-}O{-}Mn^{VII}$ = O moiety should be a weak bond.

This proposed mechanism with an ultrahigh-valent intermediate is not unprecedented. A similar mechanism involving an ultrahigh-valent $Ru^{VIII}O_4$ intermediate species has been reported for RuO_x catalysts (Giordano et al., 2016). Recently, coupling of Fe^{VI}-peroxo is also proposed as the O–O

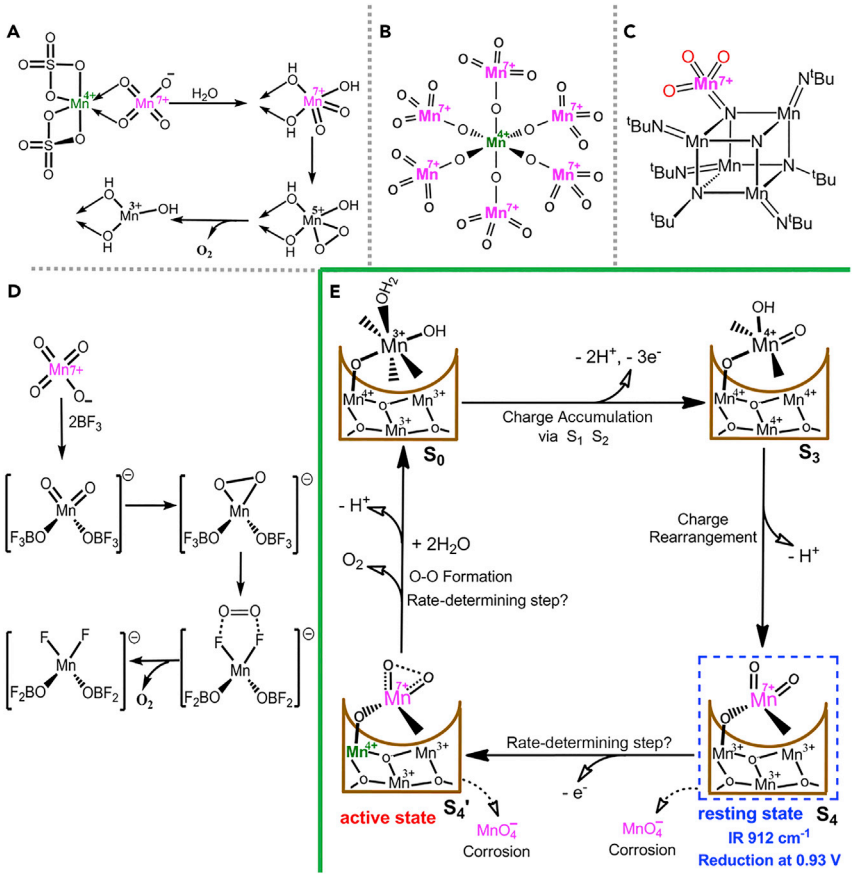

Figure 4. Proposed Catalytic Mechanism Involving Mn^{VII} = O Intermediate for Water Oxidation by MnO_x-300

(A) Pathway for oxygen evolution from MnO_4^- catalyzed by Mn^{IV} molecule (Shafirovich et al., 1981).

(B) Structure of the $[Mn^{IV}(Mn^{VII}O_4)_6]^{2-}$ complex (Krebs and Hasse, 1974). It rapidly produces O_2 at T ≥ −4°C.

(C) Structure of the cubic Mn–nitride complex (Vaddypally et al., 2017). Pendant Mn^{VII} = O moiety is preferentially reactive in comparison with free MnO_4^-.

(D) Mechanism for fast oxygen evolution from MnO_4^- with activation by a strong Lewis acid, i.e., BF_3 (Yiu et al., 2011). Oxygen evolution from 7.6 mM $KMnO_4$ completed within 200 s with the activation of 0.12 mM BF_3•CH_3CN.

(E) Proposed catalytic cycle, involving Mn^{VII} = O, in MnO_x-300-catalyzed water-oxidation reaction. The overall mechanistic process involves charge accumulation (S_0 → S_3), charge rearrangement (S_3 → S_4), active-state formation (S_4 → S_4'), and oxygen evolution (S_4' → S_0).

formation mechanism for the Ni-Fe layered double hydroxide catalyst (Hunter et al., 2018). Our proposed mechanism is consistent with the facts that the essential species Mn^{III} is always present in active Mn catalysts and that MnO_4^- is often observed in catalyst corrosion. Accordingly, we believe that, on the basis of our extensive investigations of the Mn^{VII} = O intermediate in this study, the proposed mechanism involving Mn^{VII} = O is highly probable and reliable. It offers cogent guidance for developing more efficient synthetic WOCs, and it might also be valid for the Mn_4CaO_5 cluster in PSII.

METHODS

All methods can be found in the accompanying Transparent Methods supplemental file.

SUPPLEMENTAL INFORMATION

Supplemental Information includes Transparent Methods and 15 figures and can be found with this article online at https://doi.org/10.1016/j.isci.2018.05.018.

ACKNOWLEDGMENTS

We acknowledge the financial support of this work by Swedish Energy Agency, the Knut and Alice Wallenberg Foundation, the Swedish Research Council (2017-00935), the National Natural Science Foundation of China (21120102036), and the National Basic Research Program of China (973 program, 2014CB239402).

AUTHOR CONTRIBUTIONS

B.Z. and L.S. designed the overall study. B.Z., L.F., T.L., and Q.M. performed the manganese oxide preparation and electrochemical tests. B.Z. and Q.D. carried out the *ex situ* ATR-FTIR spectroscopy measurements. B.Z. collated and analyzed data. All authors discussed the data. The manuscript was written by B.Z. and L.S.

DECLARATION OF INTERESTS

The authors declare no competing interests.

Received: April 1, 2018
Revised: May 8, 2018
Accepted: May 25, 2018
Published: June 29, 2018

REFERENCES

Abbas, H., and Nasser, S.A. (2000). Preparation and characterization of β-MnO_2-$KMnO_4$ system for battery applications. Mater. Manuf. Process. *15*, 569–580.

Baltanas, M.A., Stiles, A.B., and Katzer, J.R. (1984). An infrared spectroscopic center for catalytic science and technology study of the adsorption and surface reactions of oxygen on supported manganese oxides. J. Catal. *88*, 362–373.

Che, M., and Tench, A.J. (1983). Characterization and reactivity of molecular oxygen species on oxide surfaces. Adv. Catal. *32*, 1–148.

Chu, H.-A., Hillier, W., Law, N.A., and Babcock, G.T. (2001). Vibrational spectroscopy of the oxygen-evolving complex and of manganese model compounds. Biochim. Biophys. Acta *1503*, 69–82.

Cox, N., Pantazis, D.A., Neese, F., and Lubitz, W. (2013). Biological water oxidation. Acc. Chem. Res. *46*, 1588–1596.

Czernuszewicz, R.S., Su, Y.O., Stern, M.K., Macor, K.A., Kim, D., Groves, J.T., and Spiro, T.G. (1988). Oxomanganese(IV) porphyrins identified by resonance Raman and infrared spectroscopy. Weak bonds and the stability of the half-filled t_{2g} subshell. J. Am. Chem. Soc. *110*, 4158–4165.

Dong, J., Wang, Y., and Zhou, M. (2002). The vibrational spectrum of the MnO_2^- and MnO_4^- anions in solid argon. Chem. Phys. Lett. *364*, 511–516.

Du, H., Lo, P.K., Hu, Z., Liang, H., Lau, K.C., Wang, Y.N., Lam, W.W., and Lau, T.C. (2011). Lewis acid-activated oxidation of alcohols by permanganate. Chem. Commun. *47*, 7143–7145.

Dzhabiev, T.S. (1989). Mechanism of formation of oxygen during oxidation of water by manganese(IV) sulfate acid solutions. Kinet. Catal. *30*, 1219–1224.

Giordano, L., Han, B., Risch, M., Hong, W.T., Rao, R.R., Stoerzinger, K.A., and Shao-Horn, Y. (2016). pH dependence of OER activity of oxides: current and future perspectives. Catal. Today *262*, 2–10.

Hunter, B.M., Thompson, N.B., Müller, A.M., Rossman, G.R., Hill, M.G., Winkler, J.R., and Gray, H.B. (2018). Trapping an iron(VI) water-splitting intermediate in nonaqueous media. Joule *2*, 747–763.

Izgorodin, A., Winther-Jensen, O., and MacFarlane, D.R. (2012). On the stability of water oxidation catalysts: challenges and prospects. Aust. J. Chem. *65*, 638–642.

Jin, K., Seo, H., Hayashi, T., Balamurugan, M., Jeong, D., Go, Y.K., Hong, J.S., Cho, K.H., Kakizaki, H., Bonnet-Mercier, N., et al. (2017). Mechanistic investigation of water oxidation catalyzed by uniform, assembled MnO nanoparticles. J. Am. Chem. Soc. *139*, 2277–2285.

Krebs, B., and Hasse, K.-D. (1974). Hexamanganato(VII)manganic(IV) acid: a "pseudopermanganic acid". Angew. Chem. Int. Ed. *13*, 603.

Limburg, J., Brudvig, G.W., and Crabtree, R.H. (1997). O_2 evolution and permanganate formation from high-valent manganese complexes. J. Am. Chem. Soc. *119*, 2761–2762.

Limburg, J., Vrettos, J.S., Liable-Sands, L.M., Rheingold, A.L., Crabtree, R.H., and Brudvig, G.W. (1999). A functional model for O-O bond formation by the O_2^- evolving complex in photosystem II. Science *283*, 1524–1527.

Ma, L., Wang, Q., Man, W.L., Kwong, H.K., Ko, C.C., and Lau, T.C. (2015). Cerium(IV)-driven water oxidation catalyzed by a manganese(V)-nitrido complex. Angew. Chem. Int. Ed. *54*, 5246–5249.

Najafpour, M.M., Renger, G., Holynska, M., Moghaddam, A.N., Aro, E.M., Carpentier, R., Nishihara, H., Eaton-Rye, J.J., Shen, J.R., and Allakhverdiev, S.I. (2016). Manganese compounds as water-oxidizing catalysts: from the natural water-oxidizing complex to nanosized manganese oxide structures. Chem. Rev. *116*, 2886–2936.

Shafirovich, V.Y. (1978). Mechanism of oxygen formation in the oxidation of water by manganese(IV) sulfate. Kinetika i Kataliz *19*, 1502–1507.

Shafirovich, V.Y., Khannanov, N.K., and Shilov, A.E. (1981). Inorganic models of photosystem II of plant photosynthesis. Catalytic and photocatalytic oxidation of water with participation of manganese compounds. J. Inorg. Biochem. *15*, 113–129.

Skrabal, A. (1910). Zur selbstzersetzung der permanganate und der permangansäure. Z. Anorg. Allg. Chem. *68*, 48–51.

Takashima, T., Hashimoto, K., and Nakamura, R. (2012). Mechanisms of pH-dependent activity for water oxidation to molecular oxygen by MnO_2 electrocatalysts. J. Am. Chem. Soc. *134*, 1519–1527.

Umena, Y., Kawakami, K., Shen, J.R., and Kamiya, N. (2011). Crystal structure of oxygen-evolving photosystem II at a resolution of 1.9 Å. Nature *473*, 55–60.

Vaddypally, S., Kondaveeti, S.K., Karki, S., Van Vliet, M.M., Levis, R.J., and Zdilla, M.J. (2017). Reactive pendant Mn=O in a synthetic structural model of a proposed S_4 state in the photosynthetic oxygen evolving complex. J. Am. Chem. Soc. *139*, 4675–4681.

Walter, M.G., Warren, E.L., McKone, J.R., Boettcher, S.W., Mi, Q., Santori, E.A., and Lewis, N.S. (2010). Solar water splitting cells. Chem. Rev. *110*, 6446–6473.

Workman, J.M., Powell, R.D., Procyk, A.D., Collins, T.J., and Bocian, D.F. (1992). Vibrational

and electrochemical properties of a series of stable manganese(V)-oxo complex. Inorg. Chem. *31*, 1548–1550.

Yagi, M., and Narita, K. (2004). Catalytic O_2 evolution from water induced by adsorption of $[(OH_2)(Terpy)Mn(\mu\text{-}O)_2Mn(Terpy)(OH_2)]^{3+}$ complex onto clay compounds. J. Am. Chem. Soc. *126*, 8084–8085.

Yiu, S.M., Man, W.L., Wang, X., Lam, W.W., Ng, S.M., Kwong, H.K., Lau, K.C., and Lau, T.C. (2011). Oxygen evolution from BF_3/MnO_4. Chem. Commun. *47*, 4159–4161.

Zaharieva, I., Chernev, P., Risch, M., Klingan, K., Kohlhoff, M., Fischer, A., and Dau, H. (2012). Electrosynthesis, functional, and structural characterization of a water-oxidizing manganese oxide. Energ. Environ. Sci. *5*, 7081–7089.

Zahran, Z.N., Mohamed, E.A., and Naruta, Y. (2016). Kinetics and mechanism of heterogeneous water oxidation by α-Mn_2O_3 sintered on an FTO electrode. ACS Catal. *6*, 4470–4476.

Zandi, O., and Hamann, T.W. (2016). Determination of photoelectrochemical water oxidation intermediates on haematite electrode surfaces using operando infrared spectroscopy. Nat. Chem. *8*, 778–783.

Zhang, B., Chen, H., Daniel, Q., Philippe, B., Yu, F., Valvo, M., Li, Y., Ambre, R.B., Zhang, P., Li, F., et al. (2017). Defective and "c-disordered" Hortensia-like layered MnO_x as an efficient electrocatalyst for water oxidation at neutral pH. ACS Catal. *7*, 6311–6322.

Zhang, M., de Respinis, M., and Frei, H. (2014). Time-resolved observations of water oxidation intermediates on a cobalt oxide nanoparticle catalyst. Nat. Chem. *6*, 362–367.

ISCI, Volume *4*

Supplemental Information

Identifying Mn^{VII}-oxo Species during Electrochemical Water Oxidation by Manganese Oxide

Biaobiao Zhang, Quentin Daniel, Lizhou Fan, Tianqi Liu, Qijun Meng, and Licheng Sun

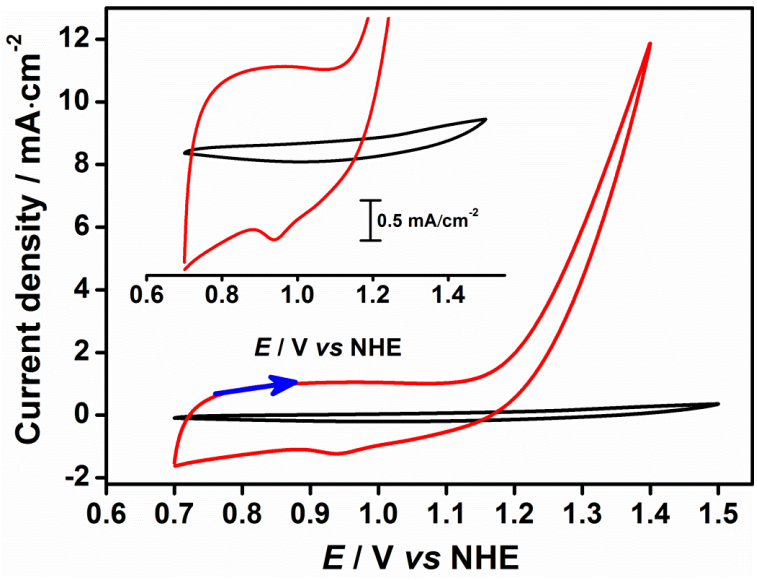

Figure S1. Comparison of CV curves of MnO_x-300 in aqueous and CH_2Cl_2 electrolyte. Related to Figure 1. CV curves of MnO_x-300 in 1.0 M KPi electrolyte (red line) and in CH_2Cl_2 with 0.1 M *n*-Bu_4NPF_6 electrolyte (black line). Scan rate 10 mV/s. The inset shows the enlarged parts of the CV curves.

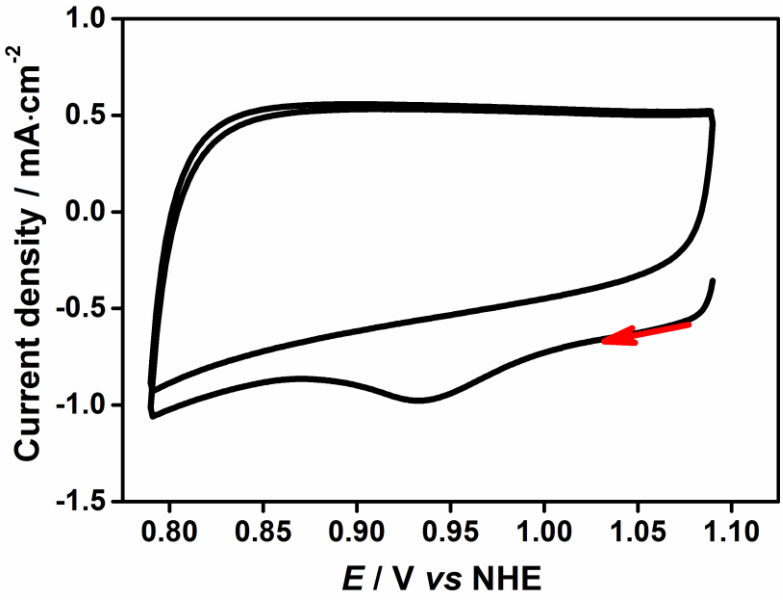

Figure S2. Electrochemical investigation on the generation of the intermediate during water oxidation. Related to Figure 1. Negative-scanned CV curves of MnO_x-300 after electrolysis at 1.4 V for 2 min. 1.0 M KPi electrolyte. Scan rate 10 mV/s.

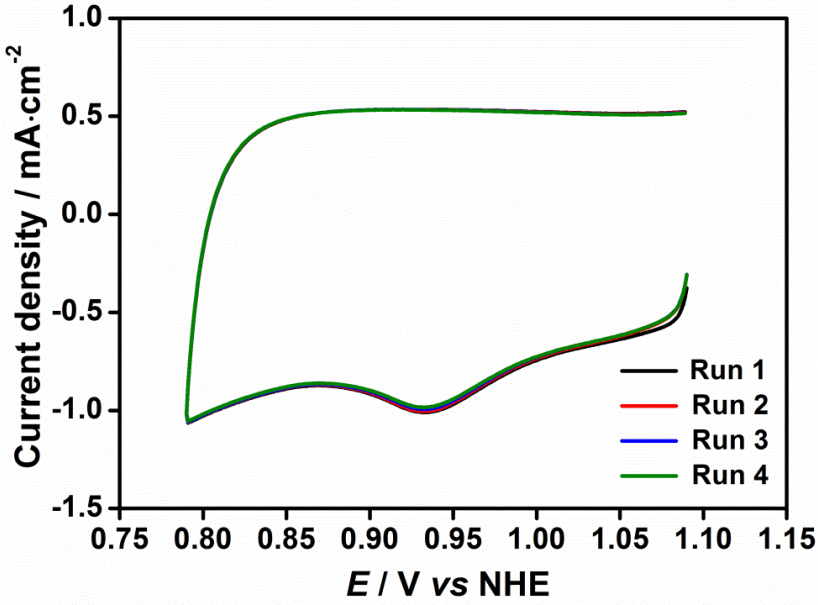

Figure S3. Electrochemical investigation on the generation of the intermediate during water oxidation. Related to Figure 1. Four repeats of negative-scanned CV curves of MnO_x-300 after electrolysis at 1.4 V for 2 min. 1.0 M KPi electrolyte. Scan rate 10 mV/s.

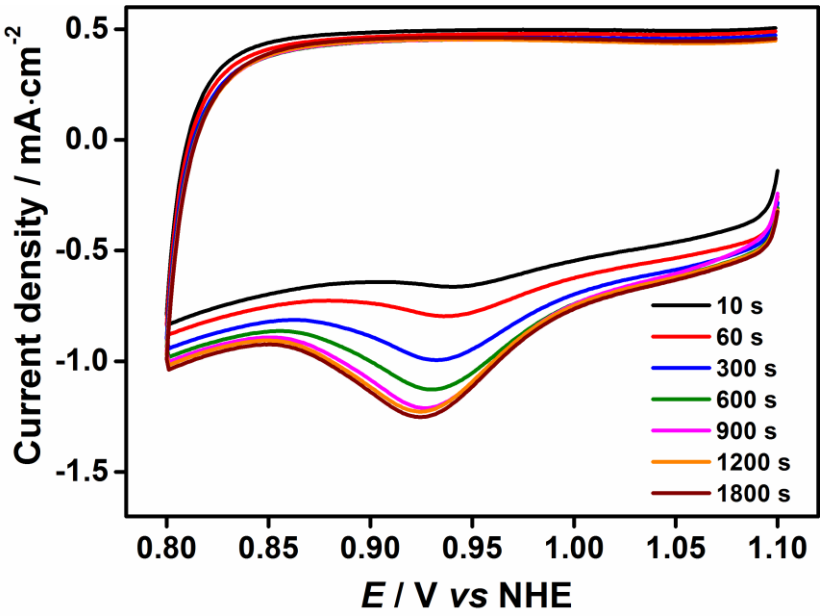

Figure S4. Electrochemical investigation on the generation of the intermediate during water oxidation. Related to Figure 1. Negative-scanned CV curves of MnO_x-300 after electrolysis at 1.4 V for different delay times. 1.0 M KPi electrolyte. Scan rate 10 mV/s.

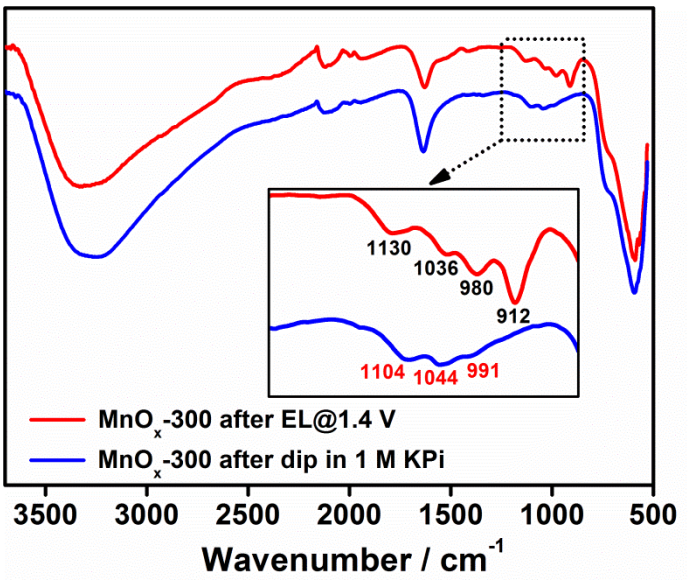

Figure S5. Assignment of the former three IR peaks at 1130 cm^{-1}, 1036 cm^{-1}, 980 cm^{-1}. Related to Figure 2. IR spectra of MnO_x-300 after electrolysis at 1.4 V and MnO_x-300 after dipping in 1.0 M KPi solution. The peaks at 1130 cm^{-1}, 1036 cm^{-1}, 980 cm^{-1} are observed for the MnO_x-300 after dipping in KPi electrolyte. However, the 912 cm^{-1} peak is completely absent.

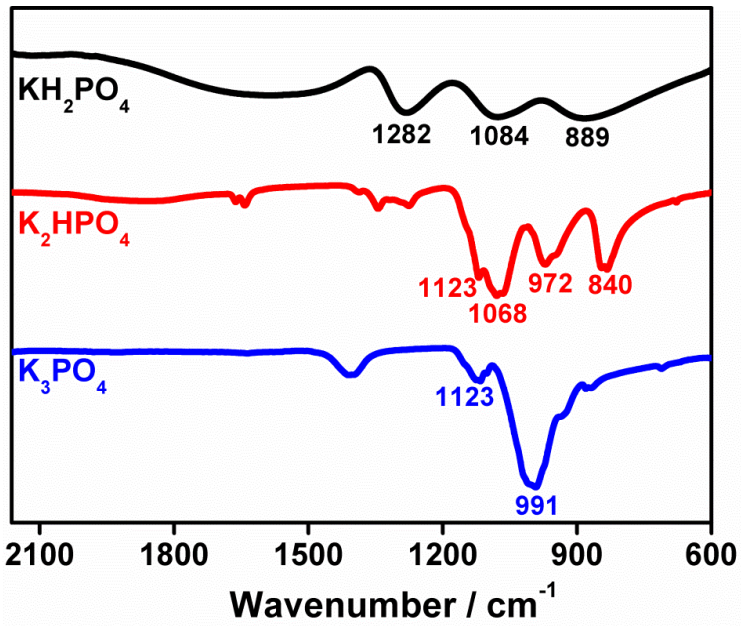

Figure S6. Assignment of the former three IR peaks at 1130 cm^{-1}, 1036 cm^{-1}, 980 cm^{-1}. Related to Figure 2. IR spectra of K_3PO_4, K_2HPO_4 and KH_2PO_4 salts. The peaks at 1130 cm^{-1}, 1036 cm^{-1}, 980 cm^{-1} are all covered in the absorption bands of phosphates.

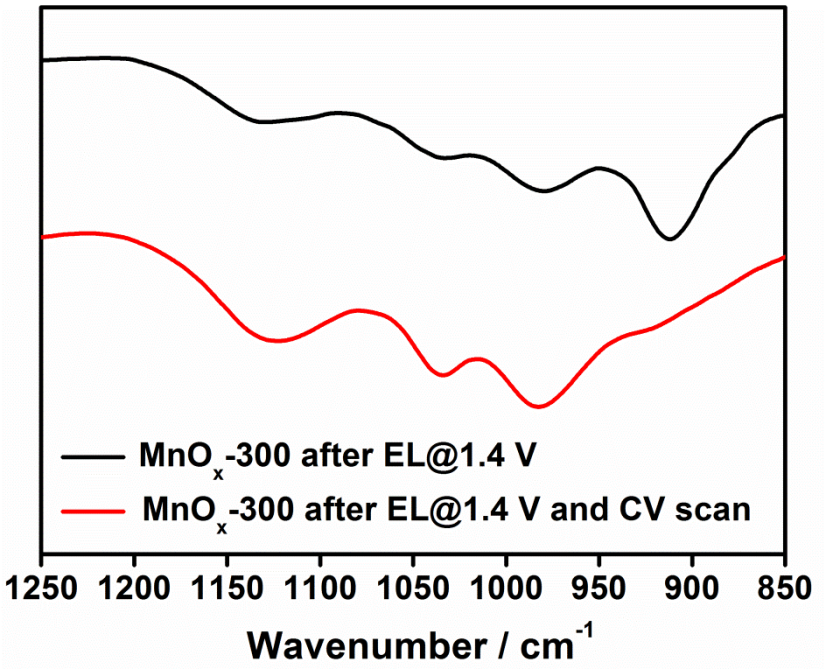

Figure S7. Related to Figure 2. IR spectra of MnO_x-300 after electrolysis at 1.4 V and MnO_x-300 after electrolysis at 1.4 V followed by negative CV scan.

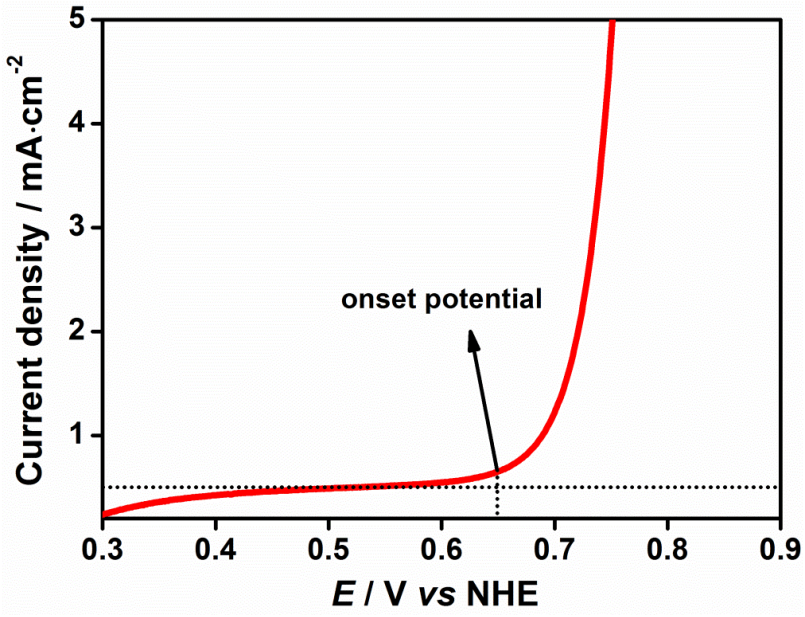

Figure S8. Related to Figure 3. LSV curves of MnO_x-300 in 1.0 M KOH. Scan rate 10 mV/s.

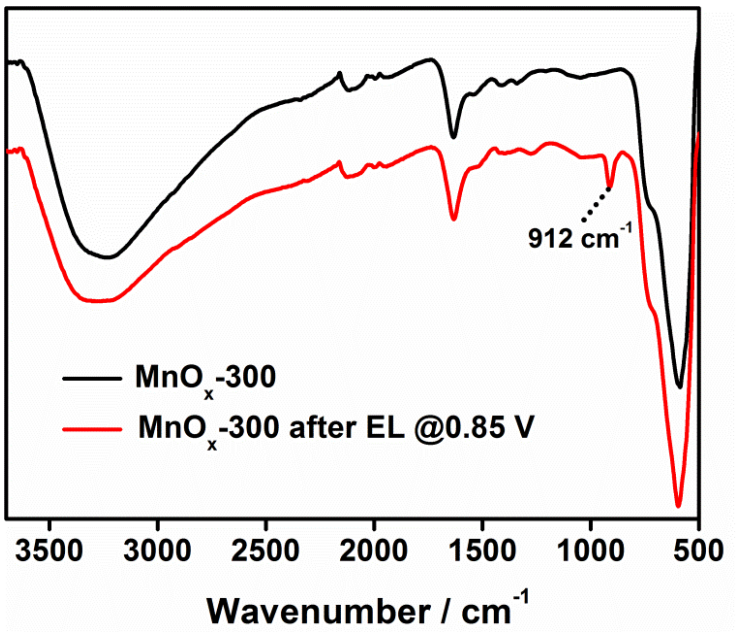

Figure S9. Related to Figure 3. IR spectra of pristine MnO_x-300 and MnO_x-300 after electrolysis at 0.85 V in 1.0 M KOH electrolyte.

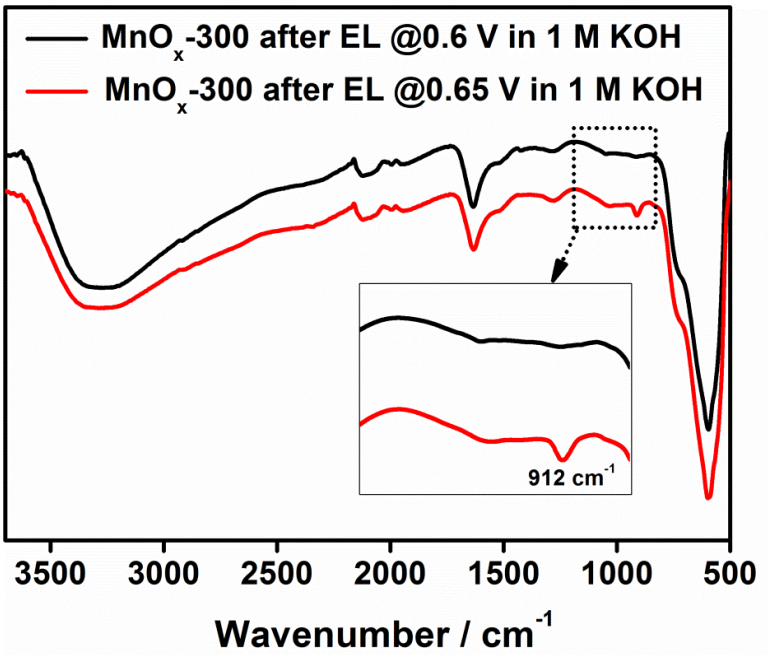

Figure S10. Related to Figure 3. IR spectra of MnO_x-300 after electrolysis at 0.6 V and 0.65 V in 1.0 M KOH electrolyte.

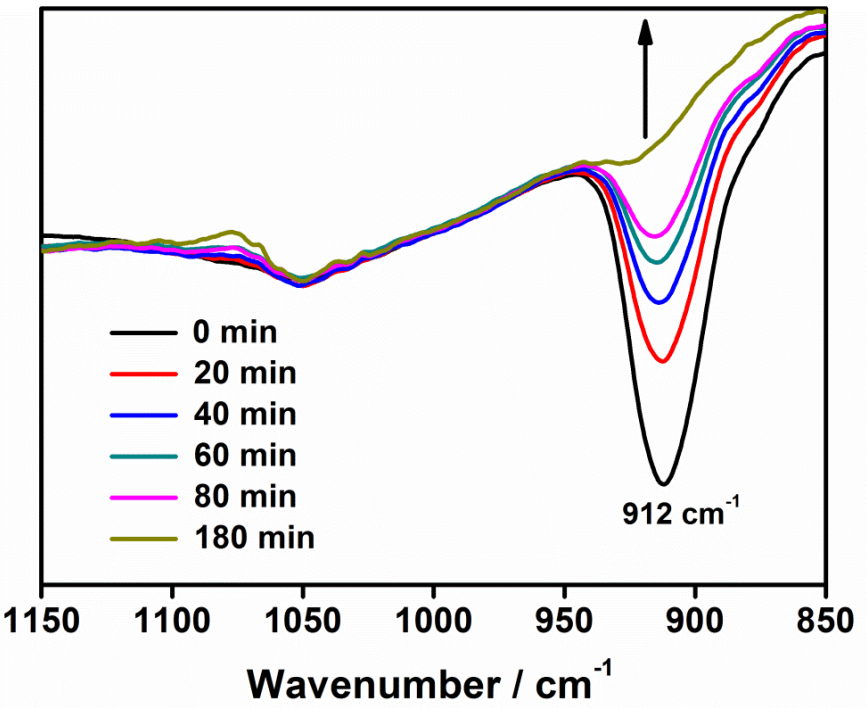

Figure S11. Related to Figure 3. Time-resolved IR spectra of MnO_x-300 after electrolysis 0.85 V in 1.0 M KOH electrolyte.

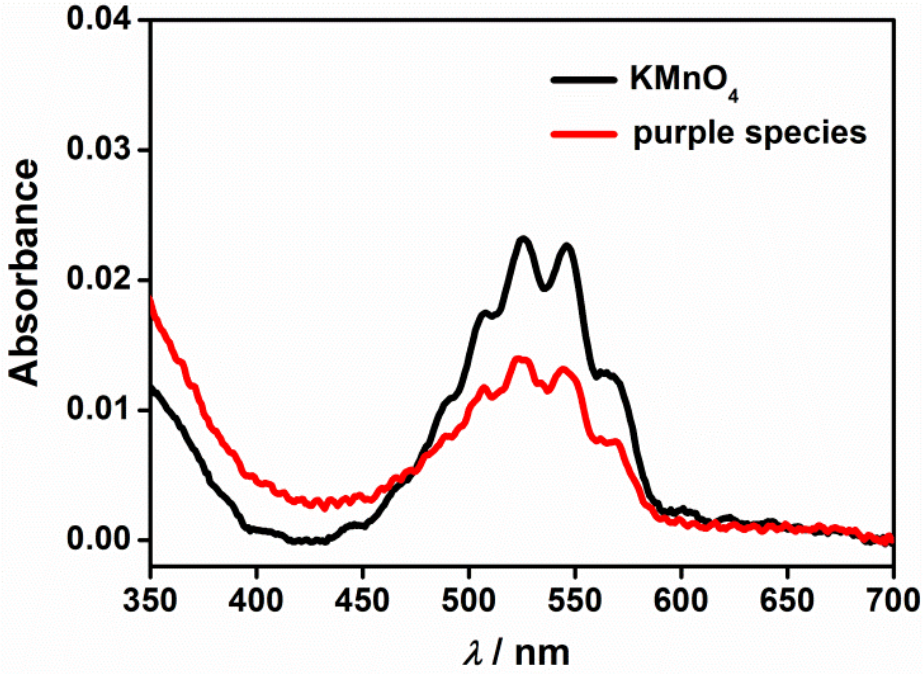

Figure S12. Related to Figure 3. UV-Vis spectra of $KMnO_4$ and the solution of the purple species from the MnO_x-300 electrode at the very first tens of seconds of electrolysis at 1.4 V.

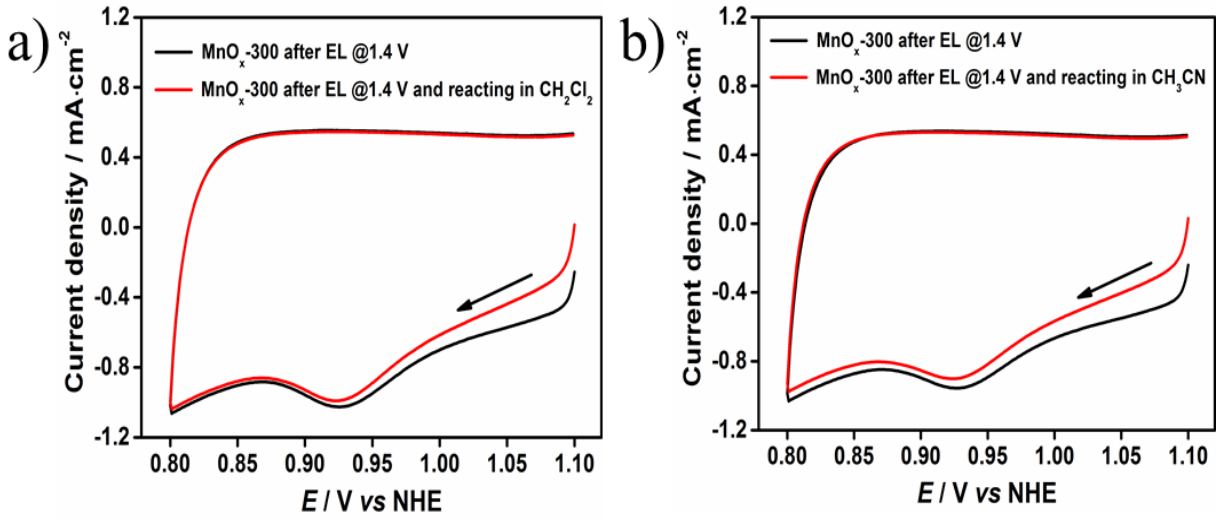

Figure S13. Related to Figure 3. Negative-scanned CV curves of MnO_x-300 after electrolysis at 1.4 V followed by reaction for 1.0 min with a) CH_2Cl_2; b) CH_3CN. 1.0 M KPi electrolyte. Scan rate 10 mV/s.

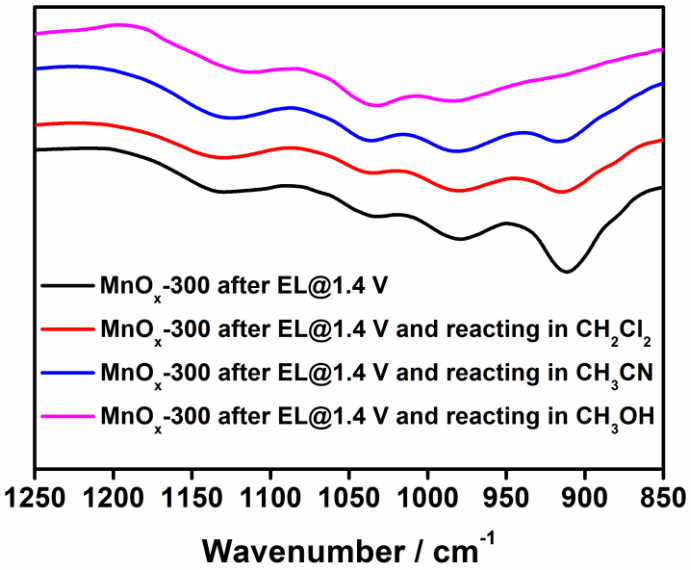

Figure S14. Related to Figure 3. IR spectra of MnO_x-300 after electrolysis at 1.4 V in 1.0 M KPi followed by reaction for 1.0 min with CH_3OH and for 5.0 min with CH_2Cl_2 and CH_3CN.

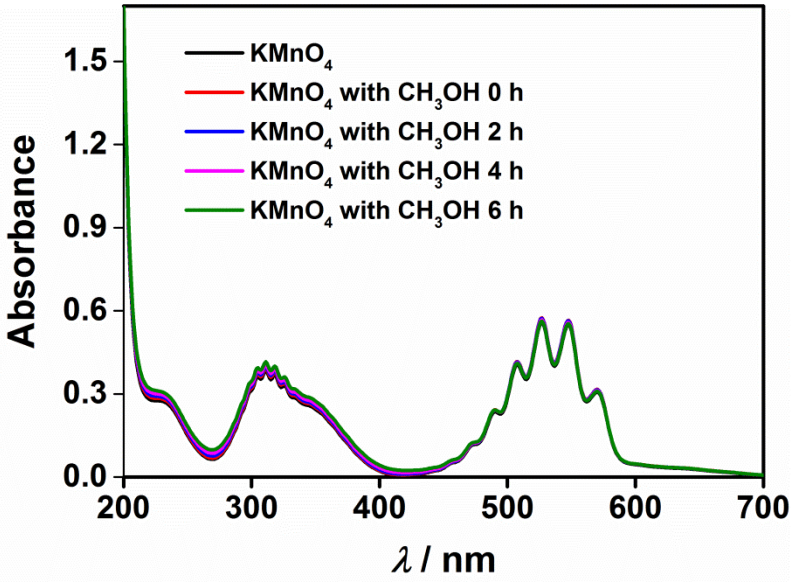

Figure S15. Related to Figure 3. UV-Vis spectra of 0.1 mM $KMnO_4$ and 0.1 mM $KMnO_4$ with 0.1 M methanol for 0 h, 2 h, 4 h and 6 h.

Transparent Methods

Materials

$Mn(CH_3COO)_2 \cdot 4H_2O$, NaCl, KH_2PO_4, K_2HPO_4, K_3PO_4, KOH, $KMnO_4$, CH_3CN, CH_3OH, CH_2Cl_2, D_2O (99.9 atom % D), 40 wt. % KOD in D_2O (98 atom % D) and $H_2{}^{18}O$ (97 atom % ^{18}O) were purchased from Sigma-Aldrich. All solvents and reagents are used as received. Ultra pure water (18.2 $M\Omega \cdot cm^{-1}$) for all the reactions or measurements was obtained from a Milli-Q system. Fluorine-doped tin oxide (FTO) substrates were purchased from Pilkington (resistance of ~8 $\Omega \cdot cm^{-2}$) and were cleaned inside an ultrasonic bath in water and ethanol for 30 min.

Preparation of MnO_x-300

The precusor manganese oxide film MnO_x-as was electro-deposited from an aqueous solution of 5 mM $(CH_3COO)_2Mn$ and 50 mM NaCl at 1.4 V for 30 minutes. Further annealing at 300 ℃ for 2 hours was performed to obtain the active MnO_x-300.

Electrochemical Measurements

All electrochemical experiments employed a CHI 650e potentiostat in a single-compartment cell with a three-electrode configuration. The cell was equipped with a FTO electrode with manganese oxide film as the working electrode, a platinum mesh as the counter electrode and an Ag/AgCl (3.5 M KCl in water) as the reference electrode. All experiments were conducted at ambient temperature (~25 ℃). All cyclic voltammograms (CV) and linear scan voltammograms (LSV) were taken with scan rate of 10 mV s^{-1}. Potential versus NHE was calibrated by using $Ru(bpy)_3Cl_2$ as a reference with $E(Ru^{II/III})$ = 1.26 V.

Infrared Spectroscopy Measurements

The attenuated total reflectance Fourier-transform infrared spectroscopy (ATR-FTIR) spectra were measured on a Thermo Scientific Nicole Is5 FT-IR spectrometer. For the general ATR-FTIR determination, manganese oxide electrodes treated after various processes were carefully rinsed by pure water and dried quickly by a N_2 flow for tens of seconds; then the manganese oxides were quickly scraped from the FTO electrode to determine their infrared absorption spectra.

Comparison of CV curves of MnO_x-300 in aqueous and CH_2Cl_2 electrolyte

When a CH_2Cl_2 solution with 0.1 M *n*-Bu_4NPF_6 was used in place of the aqueous electrolyte which is indispensable for the water oxidation reaction, there was no distinct reduction peak in the CV curve of MnO_x-300 within the potential range of 0.7-1.5 V (Figure S1).

Electrochemical investigation on the generation of the intermediate during water oxidation

After the MnO_x-300 was electrolyzed at 1.4 V for 2 min, where the catalytic water oxidation was fast, the following negative-scanned CV showed in the first cycle a large reduction peak, indicating abundance of the intermediates were formed and accumulated in MnO_x-300 during water oxidation (Figure S2). The reduction peak completely disappeared in the second cycle because the generated intermediates have been reduced in the first scanning. Repeats of the above process showed coincident CV curves. It means that the generation of the intermediate after the same process of electrolysis is repeatable (Figure S3). We also found that the formation of the intermediate needs at least 15 min to reach a saturation value along with the equilibrium of electrocatalytic water-oxidation reaction (Figure S4).

Consistency between the IR peak at 912 cm^{-1} and CV reduction peak at 0.93 V

It shows in the previous section that the CV peak of the intermediate completely vanishes after the first cycle of the negative CV scan (Figure S2). Consistently, there is no 912 cm^{-1} peak in the IR spectra of electrolyzed MnO_x-300 after negative CV scan (Figure S7). The consistency between the transient IR peak at 912 cm^{-1} and CV reduction peak at 0.93 V is further explored in the Supplementary Section 8, where the presence or absence of the IR peak at 912 cm^{-1} and the reduction peak at 0.93 V is consistent with each other and corresponds to the maintenance or degradation of the generated intermediate after reaction with different organics, respectively.

Isotopic IR spectroscopy

In order to get rid of the overlap in the IR absorption (e.g. band 1036 cm^{-1} and 980 cm^{-1}) of the phosphate group, the related catalysis by MnO_x-300 was carried out by employing 1.0 M KOH solution, in which the water-oxidation onset potential of MnO_x-300 is 0.65 V (Figure S8). In the IR spectrum of MnO_x-300 after electrolysis at 0.85 V where the rate of water oxidation is fast, 912 cm^{-1} is the only distinct new peak compared to the IR spectrum of pristine MnO_x-300

(Figure S9). The same as under neutral conditions, the 912 cm^{-1} peak only shows up when the applied potential of electrolysis is higher than onset potential of 0.65 V (Figure S10). The slow degradation of the 912 cm^{-1} peak was also observed (Figure S11). These indicate that the intermediate species involved in the catalysis under basic conditions is the same as the one revealed under neutral conditions. Therefore, it is rational to perform the isotopic IR spectroscopic study with the catalysis in KOH electrolyte solution.

1.0 M KOD-D_2O electrolyte was prepared from D_2O (99.9 atom % D) and 40 wt. % KOD in D_2O (98 atom % D). 1.0 M KOH-$H_2{}^{18}O$ electrolyte was prepared from $H_2{}^{18}O$ (97 atom % ^{18}O) and KOH. The final ratio of ^{18}O-labelled oxygen in the electrolyte is about 93%. MnO_x-300 was electrolyzed at 0.85 V in either 1.0 M KOD-D_2O electrolyte or 1.0 M KOH-$H_2{}^{18}O$ electrolyte. After electrolysis, the MnO_x-300 was carefully rinsed by either D_2O (99.9 atom % D) or $H_2{}^{18}O$ (97 atom % ^{18}O), respectively. The MnO_x-300 was then quickly dried by N_2 flow for tens of seconds. The manganese oxide was scraped off and collected for its IR spectrum.

Assignment of the 912 cm^{-1} peak

The 912 cm^{-1} peak matches with the IR absorption frequencies of $KMnO_4$, which is at 896 cm^{-1} (Figure 3c). Moreover, we did observe some purple colored species releasing from the surface of the MnO_x electrode during the very first tens of seconds of the electrolysis at 1.4 V, and then vanished in an minute (see Supplemental Video 1). The solution with the purple colored species was quickly taken out from the electrode surface and detected by UV-Vis, which clearly identified it as MnO_4^- (Figure S12). These observations prove that Mn^{VII} can be reached during water-oxidation catalysis.

Reactivity of the Mn^{VII}=O intermediate

Reactivity of the Mn^{VII}=O species on the electrolyzed MnO_x-300 was studied by reacting it with 0.1 M CH_3OH in CH_3CN. The MnO_x-300 after electrolysis at 1.4 V in KPi electrolyte was carefully rinsed by water and quickly dried by N_2 flow. Then this processed MnO_x-300 was dipped into a solution of 0.1 M CH_3OH in CH_3CN to let the generated Mn^{VII}=O species react with CH_3OH. After different reaction times, the consumptions of the Mn^{VII}=O species were determined by their negative-scanned CVs. Results show that the Mn^{VII}=O species completely vanished in one minute (Figure 3g). In the control experiments, plenty of the Mn^{VII}=O species

still remained after reaction for one minute, when the stable organics, such as pure CH_2Cl_2 and CH_3CN, were used instead of 0.1 M CH_3OH as substrate (Figure S13). The degradation and sustainment of the Mn^{VII}=O species can also be determined by its IR absorption at 912 cm^{-1} (Figure S14).

The reaction of 0.1 mM $KMnO_4$ with 0.1 M CH_3OH in CH_3CN was monitored by UV-Vis absorption, which was measured with a PerkinElmer Lambda 750 UV-Vis spectrophotometer. After even reaction for 6 h, the degradation of the $KMnO_4$ is still negligible. (Figure S15). These results support that the Mn^{VII}=O species is much more reactive than MnO_4^-.